Multivariate curve resolution with autoencoders for CARS microspectroscopy

Damien Boildieu, David Helbert, Amandine Magnaudeix, Philippe Leproux, Philippe Carré

MULTIVARIATE CURVE RESOLUTION WITH AUTOENCODER FOR CARS MICROSPECTROSCOPY

Damien Boildieu[1,2] *David Helbert*[2] *Amandine Magnaudeix*[3] *Philippe Leproux*[1] *Philippe Carré*[2]

[1] XLIM, UMR CNRS 7252, University of Limoges, France
[2]XLIM, UMR CNRS 7252, University of Poitiers, France
[3]IRCER, UMR CNRS 7315, University of Limoges, France

ABSTRACT

Coherent anti-Stokes Raman scattering (CARS) microspectroscopy is a powerful tool for label-free cell imaging thanks to its ability to acquire a rich amount of information. An important family of operations applied to such data is multivariate curve resolution (MCR). It aims to find main components of a dataset and compute their spectra and concentrations in each pixel. Recently, autoencoders began to be studied to accomplish MCR with dense and convolutional models. However, many questions, like the results variability or the reconstruction metric, remain open and applications are limited to hyperspectral imaging. In this article, we present a nonlinear convolutional encoder combined with a linear decoder to apply MCR to CARS microspectroscopy. We conclude with a study of the results variability induced by the encoder initialization.

***Index Terms*—** Multivariate curve resolution, Unmixing, CARS microspectroscopy, Autoencoders, Cell imaging

1. INTRODUCTION AND RELATED WORKS

Label-free cell imaging is the acquisition of cell images without the use of any staining, using for example fluorescent-based reagents, to locate the cell or its components of interest. One technique to acheive these acquisitions is coherent anti-Stokes Raman scattering (CARS), a vibrational spectroscopic method [1] based on a third-order non-linear optical phenomenum. Thanks to it, one can use specific frequencies to construct an image or acquire complete spectra [2, 3] allowing spectral analysis in addition to image analysis. A CARS signal intensity is composed of a resonant part and a non-resonant one. Thus, spectra are commonly processed by methods aiming to remove the non-resonant information but this can lead to introduce numerical errors. For this reason, we adress the problem of raw CARS spectra analysis.

A frequent interrogation when images composed of spectra are acquired is what are the main components in the image and what are their spectral signatures. This problem has been adressed in both chemometrics and hyperspectral imaging (HSI) communities. In chemometrics, this operation is called multivariate curve resolution (MCR) while in HSI, it is known as unmixing. As our application is CARS microspectroscopy, we use the chemometrics terminology in the remainder of this article. MCR aims to find, from a data matrix $D \in \mathbb{R}^{M \times N}$ with M acquisitions and N spectral channels, the K main components by computing their spectra $S \in \mathbb{R}^{N \times K}$ and concentrations $C \in \mathbb{R}^{M \times K}$. The problem is formulated in a linear form as follows:

$$D = CS^T + E, \tag{1}$$

with $E \in \mathbb{R}^{M \times N}$ the error matrix that contains noise and irrevelant data. MCR can be used for the analysis of microspectroscopy by unfolding the spatial dimension.

As Eq. 1 has many solutions, it is usual to apply constraints to C and S to fit to physical properties. The two most common constraints are the non-negativity and the sum-to-one ones. The first one ensures to have only positive values while the last one ensures all elements along a dimension to sum to one.

In the last years, deep learning and more particulary autoencoders (AE) became an active research field to accomplish unmixing for HSI. The flexibility of neural networks in the architecture allows a wide range of models adapted to specific of data. Hence, autoencoders cascade [4] and noise injection [5] have been used for denoising and stacked autoencoders for outliers detection [6]. Also, convolutional autoencoders [7] and multilayer decoder [8] have been used to reformulate the linear unmixing problem in a nonlinear formulation. Although several architectures have been implemented, the problem is still open. Especially since, at our knowledge, AE abilities for unmixing have never been tested in microspectroscopy.

In addition to the model structure, the choice of the loss function is a major matter as a wrong loss function will lead to incorrect components spectra. Another element to consider is the variability of the results. Indeed, as AE can have a complex structure, it is usual to initialize weights with random values. However, this can lead the training to fall in different local minima between different trainings. Moreover, this effect can be amplified by the non-resonant part of raw spectra. Therefore, studying the results variability is essential.

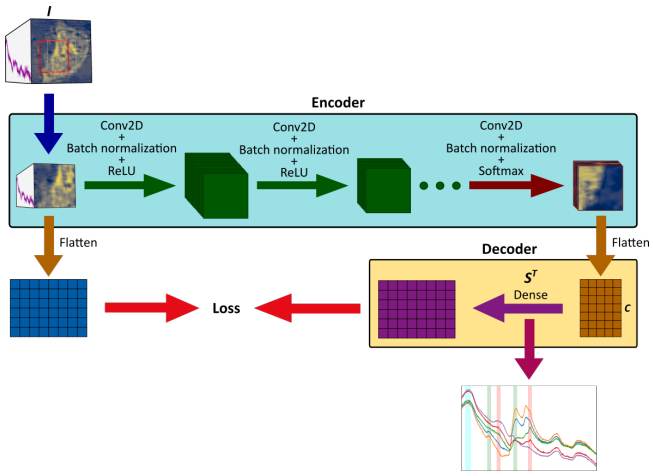

Fig. 1. Our MCR-SSAE process.

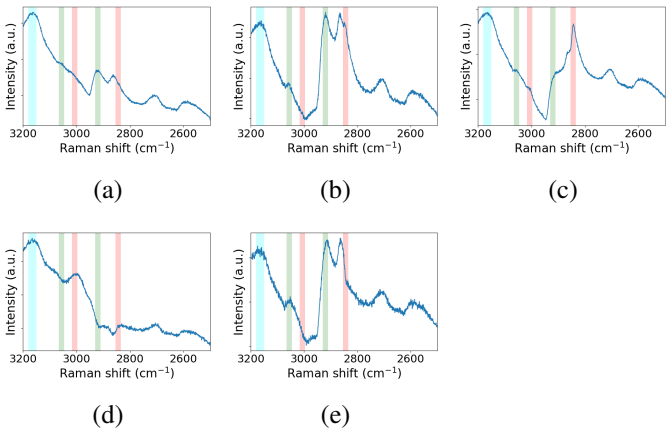

Fig. 2. Spectra obtained by the MCR-ALS. Red bands correspond to lipids, green ones to proteins and blue to water.

In this article, we introduce the use of AE for MCR in the context of CARS microspectroscopy, applied to raw CARS spectra of a cell, and we study the components spectra and concentrations variabilities along multiple trainings. First, we present the implemeted model, the training process and the hyperparametrization. Second, we introduce the dataset that will be used to evaluate our models. Third, we show the results, compare to the state of the art method and finish with studying the results variability.

2. OUR METHOD

2.1. Spectral-spatial autoencoder

Fig. 1 shows our MCR process workflow based on a spectral-spatial autoencoder (MCR-SSAE). The first block in Fig. 1 is the encoder made of several convolutional layers with non-linear activation functions. This structure allows to compute the latent space, i.e. the concentrations C with nonlinear operations and to use the spatial information in the dataset by applying spatial convolutions to every spectral channel. The second block is the decoder, a single dense layer without activation function. Hence, the decoder weights correspond to the spectra matrix S as stated in Eq. 1. We apply batch normalization (BN) between each convolution and activation function in the encoding block to smooth loss function and avoid some local minima [9], behavior that have been noticed on our data when we does not apply batch normalization. Batch normalization parameters are computed with data used for the training.

Block	Layer	Outputs	BN	Activation
Encoder	Conv5@5	16	✓	ReLU
	Conv3@3	8	✓	ReLU
	Conv1@1	5	✓	Softmax
Decoder	Dense	N	×	×

Table 1. Summary of the implemented MCR-SSAE. N is the number of spectral channels in the dataset.

We present the implemented MCR-SSAE in Tab. 1. The encoding block is made of three layers with different kernel sizes and use replication padding. The two first layers use ReLU as activation functions and the last layer uses Softmax to implement sum-to-one and non-negativity constraints. Indeed, it is usual to apply constraints on C and S matrices to ensure results consistent with their physical or numerical properties. Softmax ensures to have positive concentrations that sums to one to obtain a ratio of each component for every pixel. As both input spectra and concentrations are positive and the decoder is only a dense layer, S will also be positive.

Use spatial information requires a sufficient amount of pixels to learn spatial features but CARS acquisition are often small images. To solve this issue and increase the dataset size, we compute overlaping small patches that will be used for the training while the complete dataset is used for the inference.

2.2. Hyperparametrization

We train our model with the spectral angle distance (SAD):

$$SAD(d, \hat{d}) = acos\left(\frac{d \cdot \hat{d}}{\|d\|_2 \|\hat{d}\|_2}\right). \quad (2)$$

SAD computes similarity between spectra by computing the angle between them. We choose this function for its ability to measure the difference between the shapes of two spectra and as it already shown its efficiency in the HSI context [5]. We compute SAD between each output spectrum and its corresponding input and average it along both patches with M

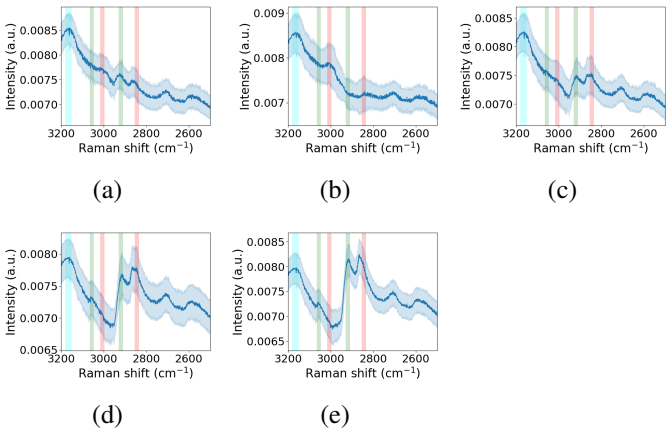

Fig. 3. Components spectra obtained by the MCR-SSAE after 50 epochs and 50 trainings. Best epoch is kept for each training. The curve is the mean and the area around the curve is the standard deviation. Red bands correspond to lipids, green ones to proteins and blue to water.

pixels and batches of size L :

$$\arg\min_{\widehat{D}} \frac{\sum_{i=1}^{L}\sum_{j=1}^{M} SAD(d_{i,j}, \widehat{d_{i,j}})}{L \times M}. \quad (3)$$

To minimize Eq. 3, we use the Adam algorithm with the initial learning rate $\alpha = 1 \times 10^{-3}$ and train for 50 epochs. These parameters have been chosen after several tests of different learning rates and number of epochs. As SAD is not magnitude sensitive, input spectra are normalized to sum to one to keep spectra with the same order of magnitude.

2.3. Decoder initialization

Finding a first guess for the component spectra is a complex operation. This first estimation can be made using spectra in the dataset that are the most subject to be composed of only one component [8, 10, 11]. In chemometrics, the simple-to-use self-modeling analysis (SIMPLISMA) method [12] is commonly used to initialize S [10]. It defines the "purity" p_i of a spectrum as $p_i = \mu_i/\sigma_i$. The first component spectrum is the spectrum with the highest p_i. The determinant of the correlation around the origin matrix is then used to correct the purity and find next spectra.

3. RESULTS

To study the ability of autoencoders to process MCR on complex dataset, we apply MCR-SSAE on coherent anti-Stokes Raman scattering (CARS) data obtained with a human embryonic kidney 293 cell (HEK293). Results are then compared to the state of the art method in chemometrics: multivariate curve analysis - alternating least squares (MCR-ALS) [10] that uses least squares regression to compute C and S. Both methods use SIMPLISMA to initialize S matrix.

CARS peaks (cm^{-1})	Assignment	Compound
2844	CH_2 s. stretch.	Lipids
2920	CH_3 s. stretch.	Proteins
3007	=C-H stretch.	Lipids
3056	aroma. C-H stretch.	Proteins
3165	O-H s. stretch.	Water

Table 2. Known vibrational bands and their associated molecular compound. s. stands for symmetrical, stretch. for stretching and aroma. for aromatic.

To study the variability of the results, we repeat 50 trainings. As we cannot be sure about the order of the found components, SAD is used to categorize found components spectra between trainings before computing any statistic.

Our implementation (available at https://gitlab.xlim.fr/boildieu1/mcr-ssae) is made in Python using PyTorch [13], MCR-ALS is implemented using pyMCR package [14].

3.1. Dataset

As explained above, the dataset is the cartography of a fixed HEK-293 cell in interphase [3] with 85×80 pixels and 916 spectral samples from 2500 to 3200 cm^{-1} acquired with a multiplex CARS (M-CARS) setup [15]. M-CARS being a method to acquire a complete spectrum in a short time. The lateral and axial resolutions are $\sim$300 nm and 2 µm and the spectral resolution is 0.8 cm^{-1}.

In the range 2500-3200 cm^{-1}, several vibrational bands are known in Raman spectroscopy and can be associated to molecular compounds [16] and, taking into account the spectral shift between Raman and CARS spectroscopy [15], can be used for CARS spectroscopy. These vibrational bands are listed in Tab. 2.

We use patches of size 30×30 pixels with a pixel overlapping of 15 pixels on both rows and columns. This size of patch allows to keep spatial details and the overlapping increase the amount of patches from 4 to 16. We chose a mini-batch approach with batches of size 3. According to our tests, the batch size is not a sensitive parameter as long as it remains low compared to the dataset size.

To select the number of components K, a pre-study based on the application of the MCR-ALS has been done. $K = 5$ was found to be appropriate.

3.2. Extracted Spectra

Fig. 2 and 3 show the components spectra found by MCR-ALS and MCR-SSAE respectively. An essential information to keep in mind when we analyze CARS spectra is that the

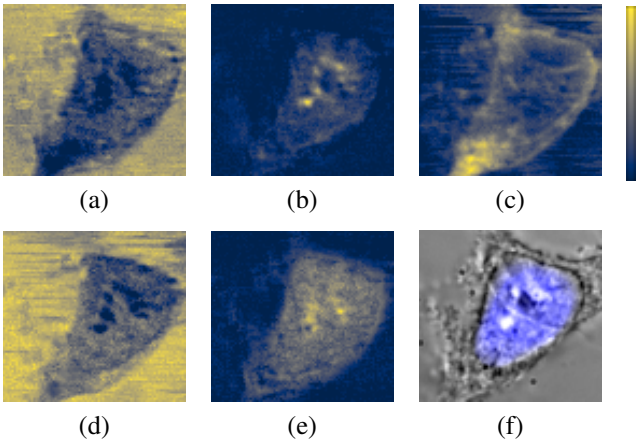

Fig. 4. Concentrations obtained by the MCR-ALS. Figure (f) corresponds to the transmitted light image of the cell and the DAPI fluorescence in blue.

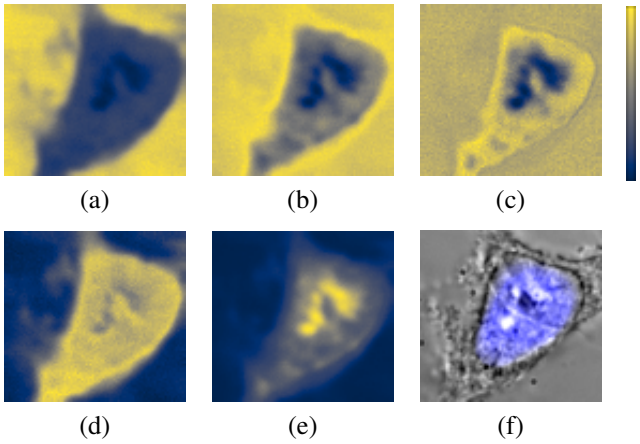

Fig. 5. Average concentrations obtained by the MCR-SSAE after 50 epochs and 50 trainings. Best epoch is kept for each training. Figure (f) corresponds to the transmitted light image of the cell and the DAPI fluorescence in blue.

vibrational information is not directly the peak but the slope of the peak, so the focus of the analysis has to be on it.

The first remark about the results is the presence of a baseline. As it is present in the input spectra and no preprocessing step is applied, it remains on the components. If we compare MCR-SSAE results to MCR-ALS ones, spectra (a) and (c) from Fig. 3 can be associated to spectrum (a) from Fig. 2 and spectrum (b) to (d). Spectra (d) and (e) extracted by MCR-SSAE correspond to spectrum (a) from MCR-ALS. Spectrum (c) in Fig. 2 does not have its equivalent in Fig. 3. Spectra (a), (b) and (c) share vibrational information at 3007 cm^{-1} and 2844 cm^{-1} highlighting lipids. Spectrum (b) differs from the other two in having no slope at 2920 cm^{-1} and spectrum (c) has a much weaker signal than spectra (a) and (b) at 3008 cm^{-1}. Spectra (d) and (e) highlight informations at 3056 cm^{-1} and have far more signifiant slopes at 2920 and 2844 cm^{-1} than spectra (a), (b) and (c).

Regarding the components spectra variability, we can see that the standard deviation is high and relatively constant along spectra. This high variation indicates that spectra highly differ along trainings.

3.3. Concentrations

In Fig. 5, we show the average concentrations obtained with the MCR-SSAE. Correspondences with the MCR-ALS results shown in Fig. 4 are not as clear as those for spectra. MCR-SSAE results are blurrier than MCR-ALS ones. As for spectra, components (a), (b) and (c) share similarities while components (d) and (e) share others. We can see components (a), (b) and (c) show th extracellular environment but gradually include elements inside the cell until component (c) that is stronger inside the cell but does not include elements inside the nucleus. Components (d) and (e) show the cell content but component (d) includes the interface while component (e) is stronger in the nucleus. An important element to note is that component (d) shows slightly parts of the cytoplasm that diffuse in the environment. This information cannot be seen in the MCR-ALS results and shows the potential of convolutional encoders to extract new informations from CARS images.

Regarding the variability, MCR-SSAE has a standard deviation that can reach 0.28, i.e. 28% of the maximum intensity. Depending of the components, this variability can be seen in the environment or the nucleus. These results indicate that found components can be more specific to a region in many trainings. This problem of variability can be attributed to 2 problems: a lack of constraint on the AE weights and a lack of spatial information to learn suitable filters.

To summarize our observations, AE are a promising tool to apply MCR on CARS spectra, allowing to extract revelant information. However, a study of results variability exhibits their present limit to deal with complex data as multiple trainings often fall into different results.

4. REFERENCES

[1] GJ Rosasco and WS Hurst, "Measurement of resonant and nonresonant third-order nonlinear susceptibilities by coherent raman spectroscopy," *Physical Review A*, vol. 32, no. 1, pp. 281, 1985.

[2] Christoph Krafft, Benjamin Dietzek, Jürgen Popp, and Michael Schmitt, "Raman and coherent anti-stokes raman scattering microspectroscopy for biomedical applications," *Journal of biomedical optics*, vol. 17, no. 4, pp. 040801, 2012.

[3] Tiffany Guerenne-Del Ben, Zakaniaina Rajaofara, Vin-

cent Couderc, Vincent Sol, Hideaki Kano, Philippe Leproux, and Jean-Michel Petit, "Multiplex coherent anti-stokes raman scattering highlights state of chromatin condensation in ch region," *Scientific reports*, vol. 9, 2019.

[4] Rui Guo, Wei Wang, and Hairong Qi, "Hyperspectral image unmixing using autoencoder cascade," in *2015 7th Workshop on Hyperspectral Image and Signal Processing: Evolution in Remote Sensing (WHISPERS)*. IEEE, 2015, pp. 1–4.

[5] Burkni Palsson, Jakob Sigurdsson, Johannes R Sveinsson, and Magnus O Ulfarsson, "Hyperspectral unmixing using a neural network autoencoder," *IEEE Access*, vol. 6, pp. 25646–25656, 2018.

[6] Yuanchao Su, Andrea Marinoni, Jun Li, Javier Plaza, and Paolo Gamba, "Stacked nonnegative sparse autoencoders for robust hyperspectral unmixing," *IEEE Geoscience and Remote Sensing Letters*, vol. 15, no. 9, pp. 1427–1431, 2018.

[7] Burkni Palsson, Magnus O Ulfarsson, and Johannes R Sveinsson, "Convolutional autoencoder for spectral–spatial hyperspectral unmixing," *IEEE Transactions on Geoscience and Remote Sensing*, vol. 59, no. 1, pp. 535–549, 2020.

[8] Mou Wang, Min Zhao, Jie Chen, and Susanto Rahardja, "Nonlinear unmixing of hyperspectral data via deep autoencoder networks," *IEEE Geoscience and Remote Sensing Letters*, vol. 16, no. 9, pp. 1467–1471, 2019.

[9] Shibani Santurkar, Dimitris Tsipras, Andrew Ilyas, and Aleksander Mądry, "How does batch normalization help optimization?," in *Proceedings of the 32nd international conference on neural information processing systems*, 2018, pp. 2488–2498.

[10] Anna De Juan, Joaquim Jaumot, and Romà Tauler, "Multivariate curve resolution (mcr). solving the mixture analysis problem," *Analytical Methods*, vol. 6, no. 14, pp. 4964–4976, 2014.

[11] Ying Qu and Hairong Qi, "udas: An untied denoising autoencoder with sparsity for spectral unmixing," *IEEE Transactions on Geoscience and Remote Sensing*, vol. 57, no. 3, pp. 1698–1712, 2018.

[12] Willem Windig and Jean Guilment, "Interactive self-modeling mixture analysis," *Analytical chemistry*, vol. 63, no. 14, pp. 1425–1432, 1991.

[13] Adam Paszke, Sam Gross, Francisco Massa, Adam Lerer, James Bradbury, Gregory Chanan, Trevor Killeen, Zeming Lin, Natalia Gimelshein, Luca Antiga, et al., "Pytorch: An imperative style, high-performance deep learning library," *Advances in neural information processing systems*, vol. 32, pp. 8026–8037, 2019.

[14] Charles H Camp Jr, "Pymcr: A python library for multivariatecurve resolution analysis with alternating regression (mcr-ar)," *Journal of Research of the National Institute of Standards and Technology*, vol. 124, pp. 1–10, 2019.

[15] Erwan Capitaine, Nawel Ould Moussa, Christophe Louot, Sylvia M Bardet, Hideaki Kano, Ludovic Duponchel, Philippe Lévêque, Vincent Couderc, and Philippe Leproux, "Fast epi-detected broadband multiplex cars and shg imaging of mouse skull cells," *Biomedical optics express*, vol. 9, no. 1, pp. 245–253, 2018.

[16] Hideaki Kano, Takumi Maruyama, Junko Kano, Yuki Oka, Daiki Kaneta, Tiffany Guerenne, Philippe Leproux, Vincent Couderc, and Masayuki Noguchi, "Ultra-multiplex cars spectroscopic imaging with 1-millisecond pixel dwell time," *OSA Continuum*, vol. 2, no. 5, pp. 1693–1705, 2019.